Ecosystems (2020) 23: 511–528
https://doi.org/10.1007/s10021-019-00416-3

ECOSYSTEMS

Dynamics of Ecosystem Water Use Efficiency in Citrus Orchards of Central India Using Eddy Covariance and Landsat Measurements

Srinivasa Rao Peddinti,[1]* B. V. N. P. Kambhammettu,[1] Suraj Reddy Rodda,[2] Kiran Chand Thumaty,[2] and Saurabh Suradhaniwar[3]

[1]*Department of Civil Engineering, Indian Institute of Technology Hyderabad, Kandi, Hyderabad, Telangana 502205, India;* [2]*National Remote Sensing Centre, Indian Space Research Organization, Hyderabad, Telangana, India;* [3]*Center of Studies in Resources Engineering, Indian Institute of Technology Bombay, Mumbai, India*

Abstract

Accurate quantification of water use efficiency (WUE) and characterization of its variability across multiple time scales can help to initiate appropriate management measures for cropland ecosystems in response to natural and anthropogenic changes. This study is aimed to understand the diurnal and seasonal patterns in WUE and its dominant controls in the citrus orchards of central India. We used eddy covariance measurements to estimate the evapotranspiration (ET) and gross primary product (GPP) fluxes from two crop cycles (2016 and 2017). On a daily scale, ET and GPP exhibited similar patterns, with peaks occurring during the fruit development stage. The daily WUE ranged from 0.22 to 3.39 g C kg^{-1} H_2O with a mean of 1.77 g C kg^{-1} H_2O. We observed high interseasonal variability in WUE, which emphasized the need to partition the fluxes between the growth stages. Landsat images were then acquired to characterize the spatiotemporal variability in WUE at the regional scale. Satellite-derived ET, GP and WUE (= GPP/ET) estimates were consistent with ground-based measurements ($R^2 > 0.80$, $n = 16$). Eight biophysical indices derived from Landsat were then regressed with WUE estimates to see whether these indices, either independently or in combination, can explain the WUE dynamics in citrus orchards. Our results indicated that the enhanced vegetation index and soil-adjusted vegetation index are strongly related to WUE with correlation strengths greater than 0.75 at all growth stages. We then developed the constitutive relations between WUE and biophysical indices that could be utilized by water managers to improve crop water productivity in response to changing agro-climatic conditions.

Key words: water use efficiency; evapotranspiration; gross primary product; citrus; eddy covariance; Landsat; METRIC; VPM.

Received 25 July 2018; accepted 22 June 2019;
published online 16 July 2019

Author's contribution Field data collection: SRP, SS; Data processing and analysis: SRP, BVNPK, SRR, KCT; Manuscript preparation: SRP, BVNPK; LANDSAT processing: SRP, SRR, KCT; Response to reviewers: SRP, BVNPK, SS.

*Corresponding author; e-mail: ce14resch01007@iith.ac.in

Highlights

- Water use efficiency fluxes were estimated for citrus orchards in central India using eddy covariance and Landsat
- Diurnal and seasonal patterns of ET, GPP, and WUE fluxes were analyzed for citrus orchards
- Role of climatic variables on ET, GPP, and WUE fluxes was investigated at ecosystem scale
- Formulated the relations between ecosystem WUE and biophysical spectral indices for use with management practices

Introduction

The exchange of carbon and water fluxes between vegetation and the atmosphere plays a crucial role in the metabolism of terrestrial ecosystems (Yu and others 2008; Ito and Inatomi 2012). These exchanges are linked through a key ecosystem characteristic called water use efficiency (WUE), which is the ratio between carbon uptake (a proxy for photosynthesis) and the accompanying water loss (a proxy for consumptive use) (Ponton and others 2006; Niu and others 2011; Song and others 2017). WUE is an indispensable eco-hydrologic trait that is used to evaluate the impact of climate change, drought, deficit irrigation, and management strategies on ecosystem productivity (Tang and others 2015b). In agronomy, WUE can be used interchangeably with crop water productivity (CWP), which is a measure of crop yield per unit of water consumed (Fan and others 2012). Sustainable agricultural practices are aimed at improving WUE or CWP by evaluating alternative management strategies to suit local agro-climatic conditions (Dar and others 2017). These improvements require a critical understanding of the yield responses to available resources and farming practices during crop growth stages (Tang and others 2015a; Qin and others 2016).

Ecosystem water use efficiency (WUE_E) is the ratio between gross primary productivity (GPP) and evapotranspiration (ET) in a relatively homogeneous terrestrial system (Law and others 2002; Reichstein and others 2007; Brümmer and others 2012). WUE_E can analyze the responses of ecosystem carbon and water balances to climate change, extreme weather conditions, and water management practices (Kuglitsch and others 2008; Niu and others 2011). WUE_E fluxes can be combined with satellite-based remote sensing data to characterize land surface exchanges at regional to global scales (Zhao and others 2007; Jung and others 2010; Tang and others 2013, 2015a). WUE_E can be accurately estimated using micrometeorological techniques such as the eddy covariance (EC) method, which considers the estimation of stomatal (photosynthesis and transpiration) and nonstomatal exchanges (respiration and evaporation) from a relatively homogeneous ecosystem (Dong and others 2011; Wagle and Kakani 2012). The EC method accurately quantifies the net exchange of heat, mass, and momentum fluxes between the surface and atmosphere by estimating the covariance of turbulent fluctuations between vertical wind (known as eddies) and the flux of interest (water vapor, CO_2, temperature, and so on). The size and shape of the flux footprint vary with measurement height, plant physical characteristics, and atmospheric stability conditions (Osmond and others 2004; Wu and others 2010). Despite its high accuracy, the estimation of WUE_E via the EC method suffers from two major shortcomings: (1) it demands expensive instrumentation for monitoring carbon and water fluxes at high frequency, and (2) it provides WUE estimates at the field scale, which is limited by the flux footprint (Ahongshangbam and others 2016).

As a cost-effective measure, satellite images along with climate data can be utilized to estimate the WUE fluxes at regional to global scales with reasonable accuracy, provided proper calibration at the flux tower is ensured (Xiao and others 2004b). The effectiveness of satellite-based ET and GPP (and hence, WUE) estimates are primarily controlled by (1) image features (such as spatial, spectral, and temporal resolutions), and (2) the method of determining the fluxes (such as energy balance, temperature-greenness, light use efficiency, spectral indicators). Moderate resolution imaging spectroradiometer (MODIS) provides direct estimates of ET and GPP at 1-km resolution averaged over an 8-day period (Zhang and others 2015). MODIS-derived GPP estimates are reliable over forest ecosystems (Xiao and others 2004a, b; Turner and others 2006; Wu and others 2010) in comparison with those over managed cropland ecosystems (Turner and others 2005; Heinsch and others 2006; Zhao and others 2007; Gitelson and others 2008). One of the several reasons for the poor performance of MODIS in cropland ecosystems is the high spatial discrepancy between the data products ($\sim 10^6$ m^2) and cropped fields (a few hundreds of m^2). A potential alternative to MODIS is the Landsat enhanced thematic mapper (Landsat—ETM+), which offers a multispectral image in 8 spectral bands at 30 m spatial resolution with a

16-day revisit interval. Landsat products can quantify the eco-physiological differences between and among the crop species, thereby reducing the uncertainties in GPP estimates (Gitelson and others 2008). A number of studies have proven the efficacy of integrated flux tower—satellite datasets in the quantification of ET (Gonzalez-Dugo and others 2009; Zhang and others 2009), GPP (Li and others 2007; Wu and others 2010; Madugundu and others 2017), and WUE (Tang and others 2015a; Zhang and others 2015) over a wide range of ecosystems. Although a few biophysical indices derived from satellite imagery (such as EVI, NDVI, and LSWI) play significant roles in regional GPP estimates, their dependency on WUE_E remains unclear (Wang and others 2010; Madugundu and others 2017). The establishment of constitutive relations and the development of correlation matrices between WUE_E and satellite-derived spectral indices can aid in evaluating alternative management scenarios for improved crop productivity.

Previous studies on characterizing WUE from citrus orchards were limited to the application of water balance techniques in conjunction with monitoring plant-based indicators. For example, Tejero and others (2011) and Consoli and others (2014) analyzed the role of deficit irrigation (DI) strategies in the WUE dynamics for citrus orchards using a number of crop physiological features. They concluded that the practice of DI strategies during flowering and fruit growth stages could have a detrimental effect on yield and fruit quality. Roccuzzo and others (2014) reported that instantaneous WUE from young orange trees could be strongly correlated with water pressure deficits. Qin and others (2016) studied the WUE dynamics in a citrus orchard through a meta-analysis using 1009 observations from 11 major citrus-producing countries and reported that the average WUE varied from 2.5 to 5 kg m^{-3}. WUE was observed to vary with the cultivation method, crop age, soil type, climatic conditions, and water and nitrogen inputs. Panigrahi and Srivastava (2017) conducted a field study on Nagpur mandarin oranges in India and observed the WUE dynamics to vary between 1.57 and 3.90 kg m^{-3} for various irrigation and fertilizer treatments. All of these studies were limited to field-scale applications and hence cannot explain the spatiotemporal variability in WUE at the regional scale caused by differences in water management practices. There is a need for additional studies that consider spatial (regional) and temporal (diurnal and seasonal) variability in WUE for an accurate understanding of the WUE fluxes in fruit crops.

To address this knowledge gap, we employ novel methods by combining EC flux measurements and high-resolution satellite data. The objectives of this study include: (1) analyze daily and seasonal patterns of WUE_E using eddy covariance measurements and quantify relationships to environmental variables, (2) estimate WUE by using METRIC and VPM models together with Landsat imagery, and evaluate with EC measurements, (3) assess spatiotemporal patterns in Landsat-derived WUE, and (4) evaluate Landsat-derived spectral indices as estimates of WUE. We adopted the mapping evapotranspiration at high resolution with internalized calibration (METRIC) and vegetation photosynthesis model (VPM) algorithms to generate spatiotemporal datasets of ET and GPP (and hence, WUE) fluxes across the region. Eight spectrally derived biophysical and environmental indices were considered to ascertain their dominance in explaining the variability in WUE so that effective management practices can be readily implemented to improve crop production.

Materials and Methods

Site Description

This study was conducted in a 30-ha citrus orchard (latitudes: 21°25′30.7″ to 21°26′2.4″E, longitudes: 78°9′30.2″ to 78°10′5.6″N, elevation: 392 m asl) located in Goregaon village of Maharashtra, India (Figure 1). The study area forms part of the Vidarbha region in central India, which is the leading producer of mandarin oranges accounting for 40% of the country's production. The crop yield of Vidarbha oranges (6.0 tons/ha) is far less than the nation's average (9.23 tons/ha); thus, the need for practicing efficient management practices is high (Peddinti and others 2018). As per the Köppen and Geiger climate classification, the region has a tropical savanna climate characterized by high temperatures and dry winter months (Kottek and others 2006). The mean annual precipitation of the region is approximately 950 mm, with humidity ranging from 35% in summer to 73% in the monsoon season. The study area is situated on the Deccan trap geologic system, which is characterized by multiple layers of solidified flood basalt resulting from volcanic eruptions. Orange trees at the experimental site had an age of 8 years, an average height of 3 m and were planted at a spacing of 5 m. The water requirements of the citrus trees are generally met through the flood system during flowering and early growth stages (for ease with fertilizer application) and through the drip system

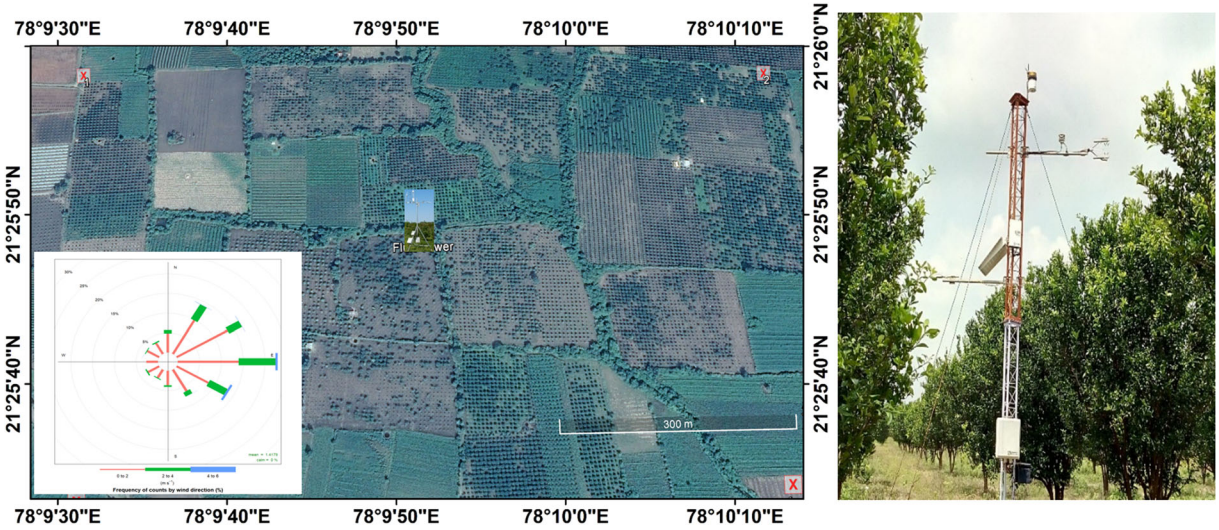

Figure 1. Typical distribution of citrus orchards in central India. The rectangular domain around the flux tower corresponds to the sub-region used for regional WUE estimation from Landsat imagery (inset: wind rose diagram). Right: flux tower installed within the study area.

during the late growth stage (due to limited resources). Irrigation scheduling is performed at 15- to 20-day intervals with an average depth of 25–35 mm. Farmers in the region intentionally water stress the crops during the pre-flowering stage to initiate blooming. The crop cycle of mandarin oranges in the study area lasts for nine months, starting from March (flowering) to November (harvest).

Flux Data Collection and Processing

The EC flux system is composed of a 3D sonic anemometer and an open-path fast response infrared gas analyzer (IRGASON-EB-IC, Campbell Sci. Inc., USA) to measure CO_2 and H_2O fluxes at a height of 5 m. Raw data were collected with a logger (CR1000, Campbell Sci. Inc., USA) at 10 Hz frequency and averaged over half-hour intervals for use with computations. Additionally, slow response meteorological variables, including precipitation (TE525-L-PTL, Tipping Bucket, Campbell Sci. Inc., USA), soil heat flux (HFP01SC-L-PT-L, Campbell Sci. Inc., USA), solar radiation (CNR 4, Campbell Sci. Inc., USA), soil moisture (CS616-L-PT-L, Campbell Sci. Inc., USA), and photosynthetically active radiation (LI-190R, LI-COR Inc., USA) were obtained at 30-min intervals. The flux tower is surrounded by a homogeneous canopy cover with similar treatment conditions (for at least 100 m in the prevailing wind direction); hence, the measured fluxes were considered representative of the entire study area.

Primary data processing was performed on half-hour mean fluxes for the period from 13 March 2016 through 25 December 2017 using Eddypro post-processing software (Version 6.2.0, LI-COR, USA). A number of standard flux corrections, including (a) removal of bad data, (b) tilt corrections on sonic measurements, (c) frequency response corrections, and (d) Webb–Pearman–Leuning (WPL) corrections, were applied on fast response measurements. The corrected fluxes exhibited spikes due to unrealistic meteorological measurements, leading to the application of secondary corrections to remove spurious data and fill the gaps with reasonable estimates. We used the REddyproc package developed in the open-source 'R' environment along with the MATLAB script to perform secondary data processing that includes: (a) flux spike removal, (b) removal of negative nighttime CO_2 fluxes, (c) friction velocity correction, and (d) gap filling and uncertainty analysis. See Rodda and others (2016) for a detailed description of the flux calculations and corrections. The corrected water vapor fluxes were correlated with vertical wind velocities to obtain actual ET from the orange fields. The corrected CO_2 fluxes were portioned into GPP and respiration by regressing reliable nighttime data with air temperature following the Lloyd and Taylor (1994) model. GPP was estimated as the difference between net ecosystem exchange (NEE) and ecosystem respiration (R_e). Finally, EC-derived ecosystem water use efficiency (WUE_{EC}) was estimated at half-hour intervals using the relation

$$\mathrm{WUE_{EC}} = \frac{\mathrm{GPP}}{\mathrm{ET}} \quad (1)$$

Landsat Data Acquisition

Advances in satellite remote sensing can provide a synoptic estimation of ecosystem fluxes over large areas with high spatial and temporal resolutions (Zhao and Running 2009; Madugundu and others 2017). The use of ETM+ sensor data from Landsat can minimize the uncertainties associated with carbon and water flux estimates and characterize WUE in the spatiotemporal domain to implement field-level management strategies (Gitelson and others 2012). Cloud-free Landsat 7 and/or 8 images encompassing the study area (path: 145, row: 045) were downloaded from the US Geological Survey (USGS) through the Earth Explorer site (http://earthexplorer.usgs.gov). The acquired images have eight spectral bands with a spatial resolution of 30 m (bands 1–7, 9), a 15-m panchromatic band (band 8), and two thermal bands with a spatial resolution of 100 m. Of the eleven bands, six bands, namely blue (B: 0.45–0.51 μm), green (G: 0.53–0.59 μm), red (R: 0.64–0.67 μm), near-infrared (NIR: 0.85–0.88 μm), shortwave infrared 1 (SWIR1: 1.57–1.65 μm), and shortwave infrared 2 (SWIR2: 2.11–2.29 μm), were used to develop biophysical indices and estimate ecosystem fluxes. A total of 16 cloud-free Landsat images, with five from the flowering stage, seven from the growth stage, and four from the harvest stage were used to estimate the WUE fluxes at regional scale following proper validation. The unavailability of satellite imagery during monsoon period due to high cloud cover has been restricted the number of images used in this study. The satellite overpass dates corresponding to the acquired images include DOY 103, and 135 in 2016 and 073, 089, and 121 in 2017 (specific to flowering), DOY 153, 199, 271, and 287 in 2016 and 153, 169, and 297 in 2017 (specific to growth), and DOY 295 and 311 in 2016 and 313 and 345 in 2017 (specific to harvest).

ET Estimation Using the METRIC Algorithm

We adopted a satellite-based METRIC algorithm coded in the open-source 'R' environment (Olmedo and others 2016) to estimate ET as a residual of energy balance at the Earth's surface, given by

$$\mathrm{LE} = R_n - G - H \quad (2)$$

where LE is latent heat flux consumed for ET ($\mathrm{Wm^{-2}}$), R_n is net radiation at the surface ($\mathrm{Wm^{-2}}$), G is the soil heat flux conducted into the ground ($\mathrm{Wm^{-2}}$), and H is sensible heat flux convected to the air ($\mathrm{Wm^{-2}}$). A brief description of the METRIC algorithm used to estimate ET is discussed herein. See Allen and others (2007) for detailed methodology and calculations.

R_n is estimated as the difference between incoming and outgoing radiant fluxes, including solar and thermal radiations, at the time of satellite overpass. G is estimated as a fraction of R_n using an empirical relation that considers surface temperature (T_s), NDVI, and albedo (Bastiaanssen 2000). The sensible heat flux (H) is estimated using the aerodynamic function at the ground surface, which is given by

$$H = \rho_{\mathrm{air}} C_p \frac{\mathrm{d}T}{r_{\mathrm{ah}}} \quad (3)$$

where ρ_{air} is the air density ($\mathrm{kg\ m^{-3}}$), C_p is the specific heat of air at constant pressure ($\mathrm{J\ kg^{-1}\ K^{-1}}$), $\mathrm{d}T$ ($= T_s - T_a$) is the near-surface temperature difference (K), and r_{ah} is the aerodynamic resistance ($\mathrm{s\ m^{-1}}$). $\mathrm{d}T$ is then linearly regressed with T_s, given by

$$\mathrm{d}T = a + bT_s \quad (4)$$

The coefficients a and b were empirically determined by computing dT at the two anchor pixels (cold and hot pixels) of the image. ET estimates from cold (well-watered vegetation) and hot (bare soil) pixels were set to minimum and maximum values of LE to estimate H at the extreme pixel locations. The ET algorithm also uses the meteorological data at the flux tower to internally calibrate the energy balance at the anchor pixels.

GPP Estimation Using the VPM Algorithm

Satellite products predominantly use light use efficiency (LUE)-based methodologies to extrapolate and scale-up site-specific GPP measurements (Prince and Goward 1996; Running and others 2000; Xiao and others 2004a). The GPP estimate from LUE models is given by

$$\mathrm{GPP} = \varepsilon_g \cdot \mathrm{FPAR} \cdot \mathrm{PAR} \quad (5)$$

where ϵ_g is LUE ($\mathrm{g\ C\ MJ^{-1}}$), PAR is the incident photosynthetically active radiation ($\mathrm{M\ Jm^{-2}}$), and FPAR is the fraction of PAR absorbed by the vegetation canopy (-). Xiao and others (2004a) found that FPAR can be partitioned into (a) photosynthetic vegetation containing leaf chlorophyll ($\mathrm{FPAR_{PAV}}$) and b) non-photosynthetic vegetation

containing senescent foliage, branches, and stems ($FPAR_{NPV}$). Replacing FPAR with $FPAR_{PAV}$ in Eq. (5) can significantly improve GPP estimates over a wide range of ecosystems with green cover (Li and others 2007; Gitelson and others 2008; Wang and others 2010; Wu and others 2010; Madugundu and others 2017). In this study, we adopted the VPM model proposed by Xiao and others (2004a) to estimate GPP from Landsat data, which is given by

$$\mathrm{GPP} = \varepsilon_g \cdot \mathrm{FPAR}_{\mathrm{PAV}} \cdot \mathrm{PAR} \tag{6}$$

A number of researchers have used satellite-derived vegetation indices as a surrogate for $FPAR_{PAV}$ when estimating GPP. Commonly used indices include NDVI (Prince and Goward 1996; Madugundu and others 2017), GCI (Gitelson and others 2008), EVI (Li and others 2007; Jiang and others 2008) and LAI (Ruimy and others 1995). Of these, EVI-based $FPAR_{PAV}$ estimates are highly reliable for cropland ecosystems (Liu and others 2014) and hence used in this study. We estimated $FPAR_{PAV}$ during the active vegetation period as a linear function of EVI, with the coefficient P set to 1.0 to minimize the parameterization (Xiao and others 2004a, b; Zhang and others 2016).

$$\mathrm{FPAR}_{\mathrm{PAR}} = \propto \times \mathrm{EVI} \tag{7}$$

Light use efficiency (ϵ_g) is estimated as a linear function of maximum LUE (ϵ_0) and downregulated factors of temperature (T_{scalar}), soil water content (W_{scalar}), and leaf phenology (P_{scalar}) on photosynthesis activity (Xiao and others 2004a, b; Madugundu and others 2017).

$$\varepsilon_g = \varepsilon_0 \times T_{\mathrm{scalar}} \times W_{\mathrm{scalar}} \times P_{\mathrm{scalar}} \tag{8}$$

The effect of temperature on photosynthesis (T_{scalar}) is estimated for each time step using the equation developed by Raich and others (1991).

$$T_{\mathrm{scalar}} = \frac{(T - T_{\min})(T - T_{\max})}{[(T - T_{\min})(T - T_{\max})] - (T - T_{\mathrm{opt}})^2} \tag{9}$$

where T_{min}, T_{max}, and T_{opt} are the minimum, maximum, and optimum temperatures for photosynthetic activity, respectively. For citrus orchards of the region, these values were obtained from flux tower data and set to 12°C, 42°C, and 28°C. The effect of soil water on plant photosynthesis (W_{scalar}) is estimated using the satellite-derived land surface water index (LSWI).

$$W_{\mathrm{scalar}} = \frac{1 + \mathrm{LSWI}}{1 + \mathrm{LSWI}_{\max}} \tag{10}$$

where $LSWI_{max}$ is the maximum LSWI across the growing season of a citrus crop for individual pixels based on the analysis of LSWI seasonal dynamics (Xiao and others 2004a, 2005). Since the citrus trees of the region have a green canopy throughout the season, the effect of leaf age on photosynthesis was considered to be maximum by setting P_{scalar} to unity.

Maximum light use efficiency (ϵ_0) was estimated by fitting a nonlinear function between net ecosystem exchange (NEE) and incident PAR at the flux tower during the peak of the plant growing season (Yan and others 2009; Wang and others 2010; Madugundu and others 2017) and is given as

$$\mathrm{NEE} = \frac{\varepsilon_0 \times \mathrm{PAR} \times \mathrm{GPP}_{\max}}{\varepsilon_0 \times \mathrm{PAR} + \mathrm{GPP}_{\max}} - R_e \tag{11}$$

where GPP_{max} is the maximum GPP estimated on a given day obtained from the EC system, and R_e is the ecosystem respiration.

Water Use Efficiency from Landsat Imagery

Pixel-to-pixel algebraic operations were performed on Landsat-derived GPP and ET products to estimate WUE following Eq. (1). This process also enabled us to understand the spatial patterns in WUE in response to field-level resource availability and management operations. The efficacy of using Landsat imagery to capture the WUE dynamics at the flux tower was evaluated using residual statistical parameters. The temporal WUE patterns were then analyzed to comment on intra- and interseasonal fluctuations.

Spectral Indices from Landsat Imagery

As ET (from METRIC), GPP (from VPM), and hence WUE estimations are computationally exhaustive and demand a large number of parameters, we tried to identify the biophysical spectral indices with the greatest influence that could explain the WUE variations for different growth stages. Eight spectral indices derived from Landsat imagery were considered to investigate their ability to explain the WUE_E dynamics and constitute functional relations. This evaluation can aid in estimating WUE_E directly from the dominant indices so that efficient management activities in response to dynamic changes in WUE can be readily implemented. For each image, site-specific pixels corresponding to a rectangular domain of 3.6 km^2 (20 × 20 pixels) with the flux tower at the center were extracted (Kalfas and others 2011; Souza and others 2014;

Danelichen and others 2015; Kang and others 2016; Madugundu and others 2017). The spectral indices used in this study include the following:

1. Normalized difference vegetation index (NDVI)—a measure of vegetation productivity of terrestrial ecosystems, given by Rouse and others (1973)

$$\mathrm{NDVI} = \frac{\rho_{\mathrm{nir}} - \rho_{\mathrm{red}}}{\rho_{\mathrm{nir}} + \rho_{\mathrm{red}}} \tag{12}$$

2. Enhanced vegetation index (EVI)—a measure of vegetation productivity adjusted for residual atmospheric correction, soil and canopy background reflectance, given by Huete and others (1997)

$$\mathrm{EVI} = 2.5\left(\frac{\rho_{\mathrm{nir}} - \rho_{\mathrm{red}}}{[\rho_{\mathrm{nir}} + (6\rho_{\mathrm{red}} - 7.5\rho_{\mathrm{blue}}) + 1]}\right) \tag{13}$$

3. Soil-adjusted vegetation index (SAVI)—a measure of vegetation productivity that minimizes the influence from soil brightness, given by Huete (1988)

$$\mathrm{SAVI} = \frac{(1+L)(\rho_{\mathrm{nir}} - \rho_{\mathrm{red}})}{(\rho_{\mathrm{nir}} + \rho_{\mathrm{red}} + L)} \tag{14}$$

where 'L' is the canopy background adjustment factor, which varies from 0 (no vegetation) to 1 (full vegetation). A value of 0.5 for L is considered in this study.

4. Green-NDVI (GNDVI)—a measure of vegetation productivity considering chlorophyll concentration, given by Gitelson and others (1996)

$$\mathrm{GNDVI} = \frac{\rho_{\mathrm{nir}} - \rho_{\mathrm{green}}}{\rho_{\mathrm{nir}} + \rho_{\mathrm{green}}} \tag{15}$$

5. Green chlorophyll index (GCI)—a measure of vegetation productivity considering leaf area index, given by Gitelson and others (2003)

$$\mathrm{GCI} = \frac{\rho_{\mathrm{nir}}}{\rho_{\mathrm{green}}} - 1 \tag{16}$$

6. Simple ratio (SR)—a measure of high vegetation productivity with reduction in atmosphere and topography effects, given by Jordan (1969)

$$\mathrm{SR} = \frac{\rho_{\mathrm{nir}}}{\rho_{\mathrm{red}}} \tag{17}$$

7. Specific leaf area vegetation index (SLAVI)—a measure of leaf canopy linked with plant ecophysiology and leaf biochemistry, given by Lymburner and others (2000)

$$\mathrm{SLAVI} = \frac{\rho_{\mathrm{nir}}}{\rho_{\mathrm{red}} + \rho_{\mathrm{swir2}}} \tag{18}$$

8. Land surface water index (LSWI)—a measure of liquid water in vegetation canopies, given by Xiao and others (2004b)

$$\mathrm{LSWI} = \frac{\rho_{\mathrm{nir}} - \rho_{\mathrm{swir1}}}{\rho_{\mathrm{nir}} - \rho_{\mathrm{swir1}}} \tag{19}$$

where the notation ρ_X stands for the spectral reflectance in band 'X'.

Results

Environmental Conditions

The temporal patterns of all climatic variables displayed similar trends between the crop cycles (Figure 2). The maximum, minimum, and mean daily values of air temperature, VPD, and solar radiation during the monitoring period were observed to be 47°C, 11.5°C, and 26.5°C; 6, 0.46, and 2.36 kPa; and 854, 54, and 223 Wm^{-2}, respectively. Air temperature and solar radiation peaked in May and gradually decreased thereafter (Figure 2A, C). Starting from the onset of the monsoon season (June), VPD decreased drastically due to the increases in precipitation and humidity. Total precipitation of 300 mm (and 570 mm) was recorded during the monsoon of 2016 (and 2017), which is approximately 63% (and 29%) less than the mean monsoon rainfall for the study region (Figure 2D). Soil moisture was low during flowering to the early fruit development stage (March-June) but gradually increased in the fruit growth and ripening stages (July-October), with an average value of 0.39 $\mathrm{cm}^3\ \mathrm{cm}^{-3}$, which is slightly less than the field capacity and represents a condition favorable for citrus fruit growth (Figure 2E). The relative humidity was high in the months of July and August, with maximum values of 60% in 2016 and 80% in 2017 (Figure 2F). The LAI gradually increased from an average of 2.4 $\mathrm{m}^2\ \mathrm{m}^{-2}$ at the flowering stage to an average of 5.6 $\mathrm{m}^2\ \mathrm{m}^{-2}$ at the ripening stage.

Seasonal Variations in ET, GPP, and WUE

GPP and ET exhibited similar patterns starting with low water consumption (1.98 ± 0.98 mm m^{-2} day^{-1}) and production rates (2.55 ± 1.9 g C m^{-2} day^{-1}) during the flowering and early growth stages (March-June), with an increase to a peak during the fruit development and ripening stages (3.26 ± 1.84 mm m^{-2} day^{-1} and 6.14 ± 3.91 g C m^{-2} day^{-1}), followed by a decreasing trend during the harvest stage (2.56 ± 0.74 mm m^{-2} day^{-1} and

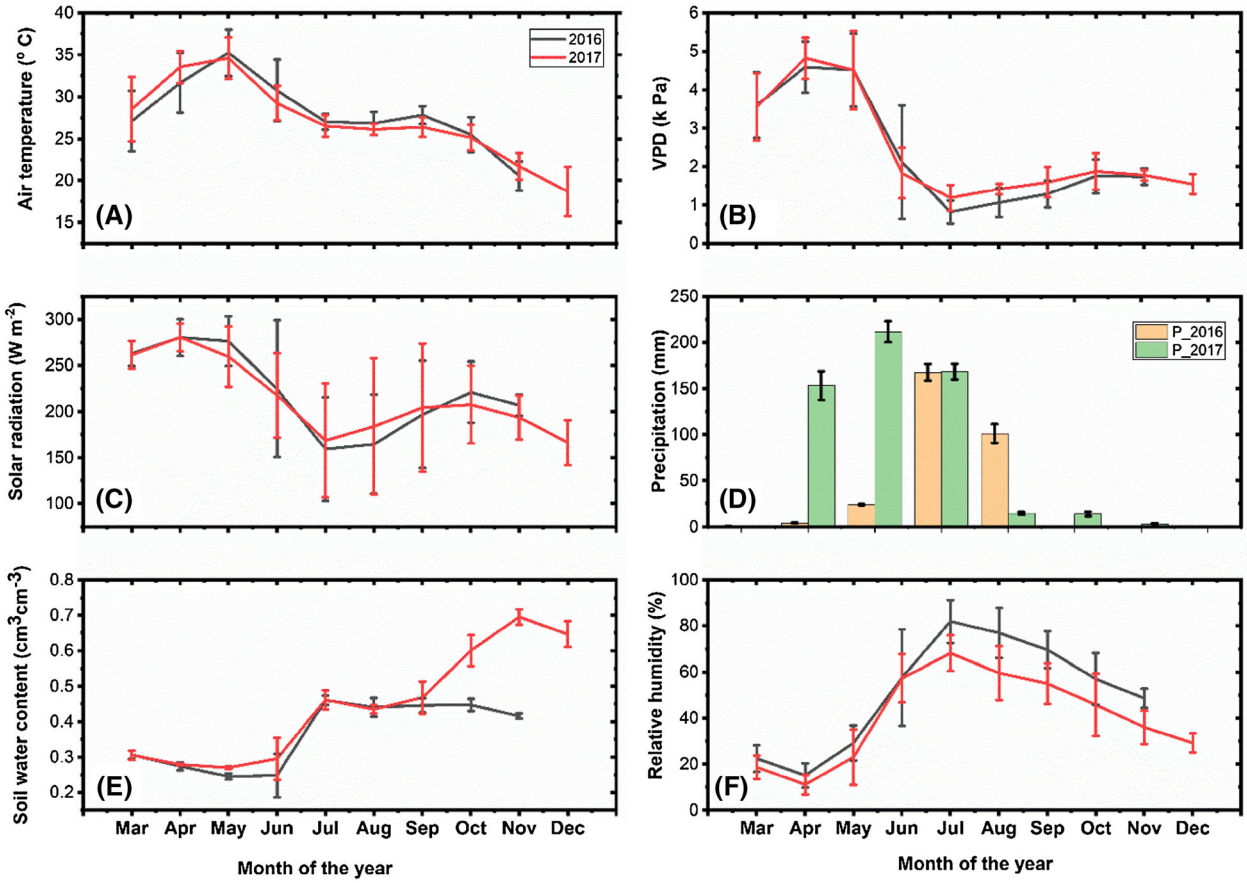

Figure 2. Seasonal variations of monthly means of **A** air temperature, **B** vapor pressure deficit, **C** solar radiation, **D** precipitation, **E** soil water content, and **F** relative humidity observed at the flux tower during the citrus crop cycles of 2016 and 2017

4.86 ± 0.80 g C m^{-2} day^{-1}) (Figure 3A, B). Similarly, WUE was low during the flowering stage (1.46 ± 1.51 g C kg^{-1} H_2O) and peaked during the fruit development stage (2.49 ± 1.09 g C kg^{-1} H_2O), followed by a slight reduction during the harvest stage (2.01 ± 0.62 g C kg^{-1} H_2O) (Figure 3C). To divulge the role of climate variables on atmospheric carbon and water fluxes, we regressed the monthly mean ET and GPP fluxes with various environmental factors (Figure 4). At the monthly scale, both ET and GPP were fitted linearly with relative humidity, whereas the fit with other parameters was nonlinear. The monthly averaged ET and GPP fluxes exhibited distinct nonlinear trends with solar radiation, air temperature, soil moisture, and VPD (Figure 4). This finding reveals that seasonal variability in major climate variables drives photosynthesis and transpiration rates with varying strengths (Yu and others 2008; Tong and others 2014a; Liu and others 2017). Similarly, the role of climate variables on the coupled carbon-water fluxes (that is, WUE) was evaluated by linearly regressing WUE with environmental factors (Figure 5). WUE is positively correlated with soil water content and precipitation, whereas WUE is negatively correlated with VPD, solar radiation, and air temperature.

Diurnal WUE Fluxes in Citrus Orchards

To understand the plant photosynthesis and transpiration responses to rapid changes in meteorological parameters, we analyzed the diurnal variations in WUE during the crop cycle. The diurnal trends in WUE were identical between the crop stages with two peaks, one occurring in the morning (1.85 ± 0.64 g C kg^{-1} H_2O) and the other in the evening (1.76 ± 1.36 g C kg^{-1} H_2O) with a low steady-state WUE in between (0.87 ± 0.17 g C kg^{-1} H_2O) (Figure 6). The diurnal patterns in WUE among the growth stages indicate that the highest magnitude and amplitude (maximum minus minimum) in WUE were observed during the post-harvesting followed by the fruit development

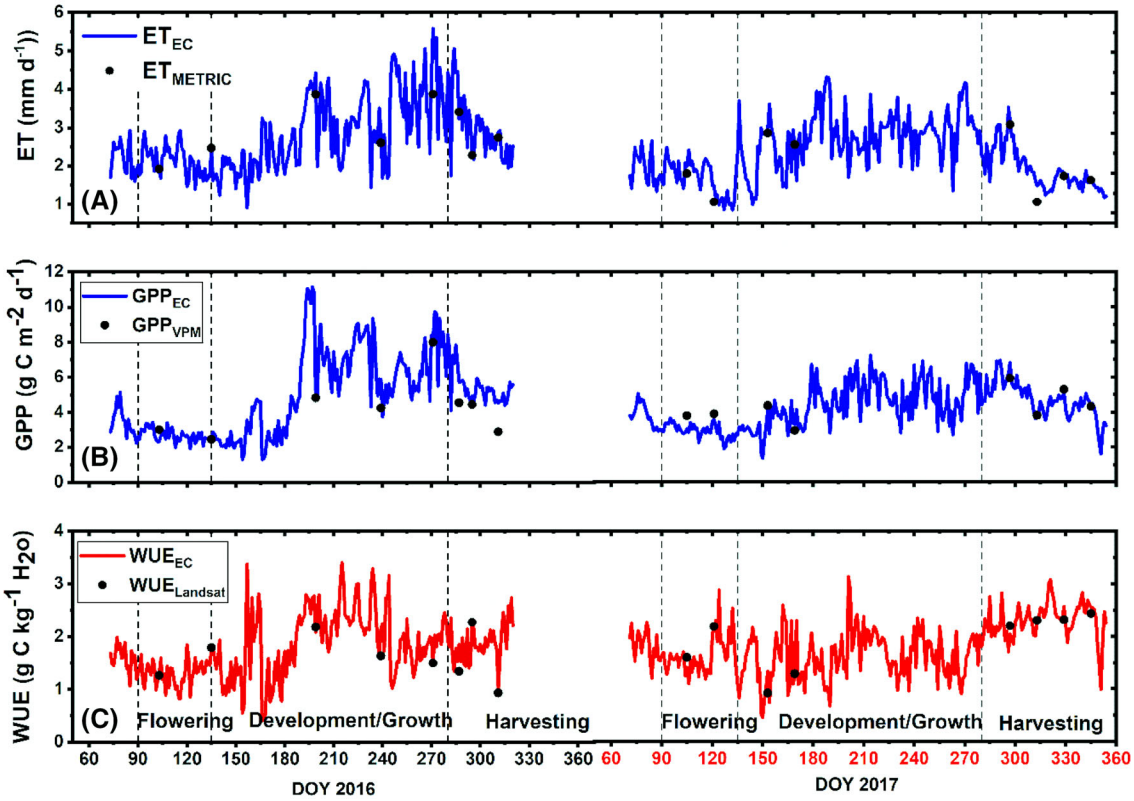

Figure 3. Seasonal variations of daily **A** evapotranspiration (ET), **B** gross primary product (GPP), and **C** water use efficiency (WUE) derived from flux tower measurements. Landsat-derived fluxes for the dates of satellite overpass at the pixel containing the flux tower were represented using dots (·) for ease with the comparison (crop stages considered include: flowering: April–June, growth: July–October, and harvest: November–December).

stages. During early morning hours of the day (06:00–08:00 am), a sharp increase in solar radiation (0–62 Wm^{-2}) augments stomatal conductance, resulting in increased photosynthesis and WUE. As the time of the day progresses, a decrease in GPP due to stomatal closure combined with an increase in ET due to increased VPD (10–26 kPa) results in low WUE fluxes. Just before the sunset, a reduction in solar radiation and air temperature results in a sharp decrease in ET, which is much higher than the increase in GPP, resulting in increased WUE. The diurnal courses of WUE in the citrus orchards of the study region are in agreement with those in the managed croplands of similar agro-climatic zones (Tong and others 2009, 2014a).

Landsat Evaluation of ET, GPP, and WUE Fluxes

The Landsat-derived fluxes for the pixel containing the flux tower location were validated with EC measurements for the days of satellite overpass (Figure 7). This comparison is meaningful because the flux footprint is completely contained by the image boundary, satisfying the condition of homogeneity. Good correlations between the EC-measured and Landsat-derived ET (R^2 = 0.84), GPP (R^2 = 0.82), and WUE fluxes (R^2 = 0.82) were reported, confirming the effectiveness of Landsat-based estimation methodologies to characterize the spatiotemporal variability in ET, GPP, and hence WUE fluxes at the regional scale.

Spatial Distribution of WUE Fluxes

Following validation with EC flux data, Landsat imagery was utilized to upscale EC flux measurements and characterize spatial variability in WUE fluxes (Figure 8). Farmers of the region practice different irrigation and management strategies, to attain the trade-off between the amount of irrigation water supplied and crop production. Hence, spatial variability in WUE is obvious during the crop cycle. Spatial variability in WUE is low during

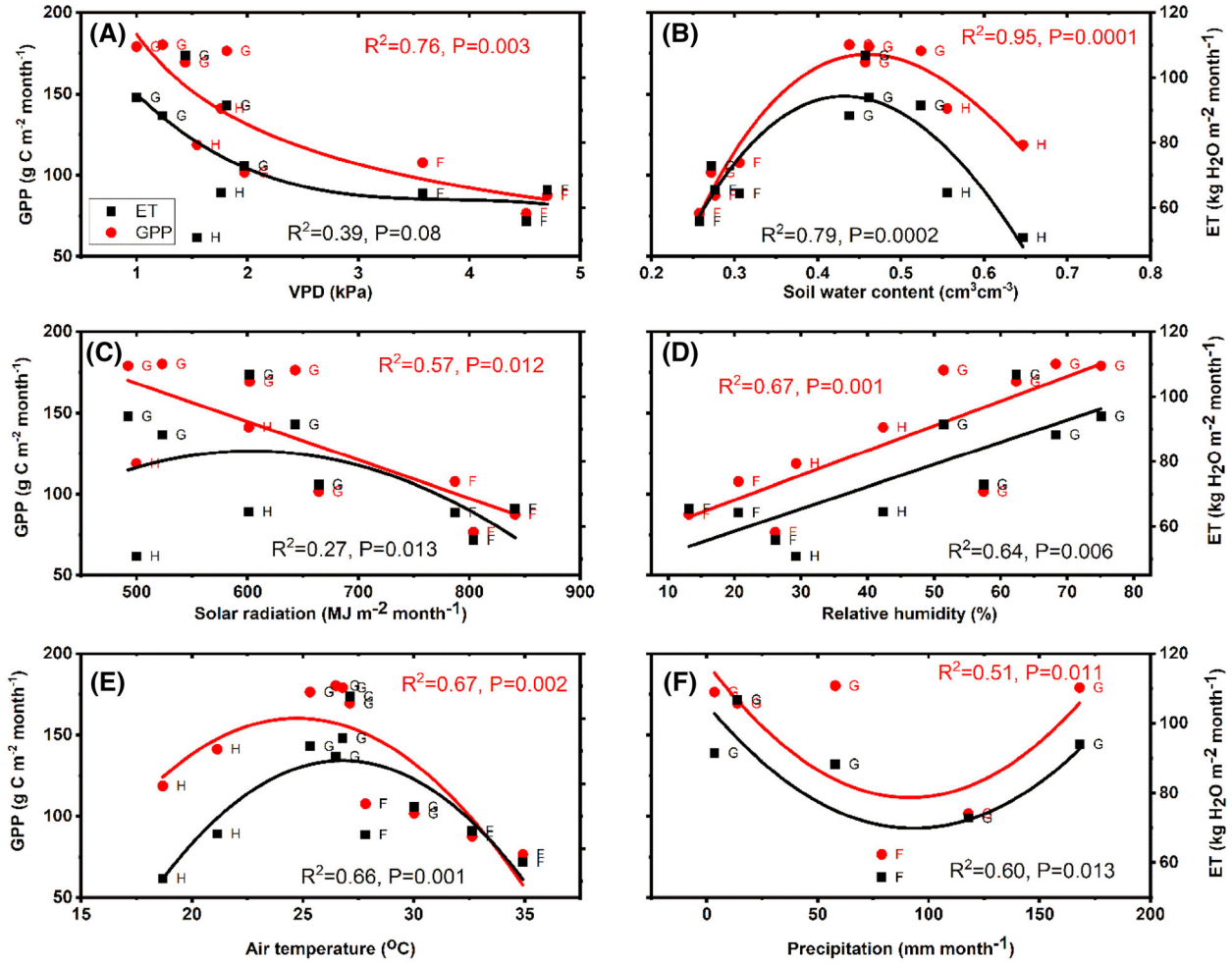

Figure 4. Relationship of monthly mean gross primary productivity (GPP) and evapotranspiration (ET) with monthly means of **A** vapor pressure deficit, **B** soil water content, **C** solar radiation, **D** relative humidity, **E** air temperature, and **F** monthly cumulative precipitation for the citrus orchards. All calendar months are represented using crop growth stages with 'F' indicating flowering stage, 'G' indicting fruit development or growth stage, and 'H' indicating harvesting stage of the citrus crop cycle.

the pre-flowering stage, as almost all farmers intend to water stress the crop to initiate blooming. During the flowering and early growth stages (DOY < 140), uniform fertilizer application with flood irrigation resulted in a fairly homogeneous distribution of WUE across the region (0.94 ± 0.02 g C kg^{-1} H_2O). Spatial anomalies in WUE were observed during the crop development stage, as the frequency and amount of irrigation during this period are governed by the availability of resources. Large spatial variability during harvest (DOY > 270) could be attributed to a large number of fragmented lands, wherein the farmers' intuition played a significant role in selecting the harvesting method and date specific to the farm. The northern and southeastern regions of the study area (Figure 8) consistently recorded high WUE due to the availability of resources to cope with the water stress conditions.

WUE Variability with Spectral Indices

We considered eight biophysical spectral indices (that is, NDVI, EVI, SAVI, GNDVI, GCI, SR, SLAVI, and LSWI) that can be readily derived from Landsat spectral reflectance data to determine whether these indices can explain the WUE dynamics. All the indices exhibited a positive correlation with WUE fluxes during the flowering, development, and harvesting stages (Figure 9). The WUE values

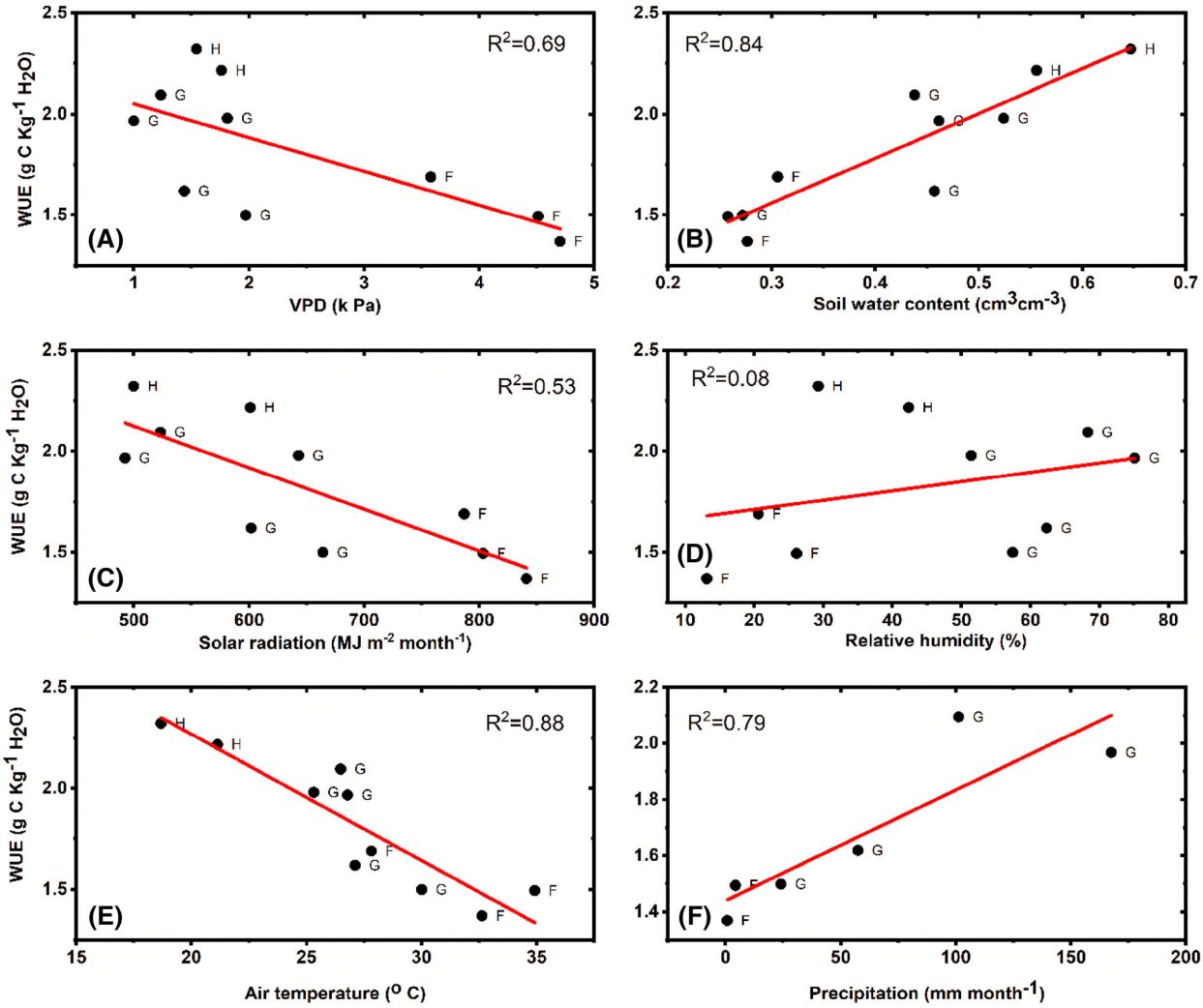

Figure 5. Relationship of monthly mean ecosystem water use efficiency (WUE) with monthly means of **A** vapor pressure deficit, **B** soil water content, **C** solar radiation, **D** relative humidity, **E** air temperature and **F** monthly cumulative precipitation for the citrus orchards. All calendar months are represented using crop growth stages with 'F' indicating flowering stage, 'G' indicting fruit development or growth stage, and 'H' indicating harvesting stage of the citrus crop cycle.

ranged from 0.62 to 2.8 g C $kg^{-1}H_2O$ during the flowering stage, 0.65–4.2 g C $kg^{-1}H_2O$ during the development stage, and 0.73–4.1 g C $kg^{-1}H_2O$ during the harvesting stage (Figure 9). During the crop cycle, the EVI values ranged from 0.1 to 0.6, the NDVI values ranged from 0.2 to 0.79, the GCI values ranged from 1 to 6.8, the LSWI values ranged from − 0.5 to 0.45, the GNDVI values ranged from 0.25 to 0.75, the SAVI values ranged from 0.1 to 0.65, the SLAVI values ranged from 0.5 to 3.8, and the SR values ranged from 2 to 12. These indices exhibited different correlation strengths with WUE at different crop stages (Figure 8). Of these, two indices, EVI and SAVI showed strong linear dependency with the WUE fluxes at all growth stages with $R^2 > 0.75$ (Table 1).

Discussion

Impact of Environmental Variables on GPP, ET, and WUE

We observed strong negative correlations between VPD and ET and between VPD and GPP, which disagrees with the results of previous studies (Liu and others 2014, 2017; Tong and others 2014a). However, the asynchronous response of these fluxes resulted in a decreasing trend in WUE with an increase in VPD, concurring with previous studies specific to cropland ecosystems in a tropical savannah climate (Figure 5). This result could be due to the different vegetation phenology and management activities being practiced by the farmers in the region, which demand less irrigation

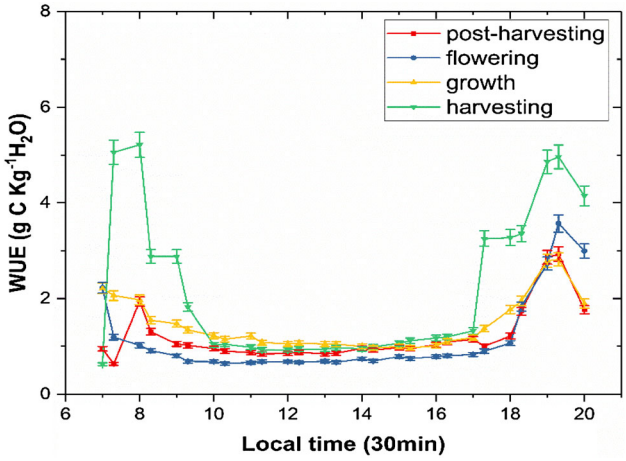

Figure 6. Diurnal variations in water used efficiency (WUE) during different growth stages of the citrus crop (crop stages considered include: flowering: April–June, growth: July–October, and harvest: November–December).

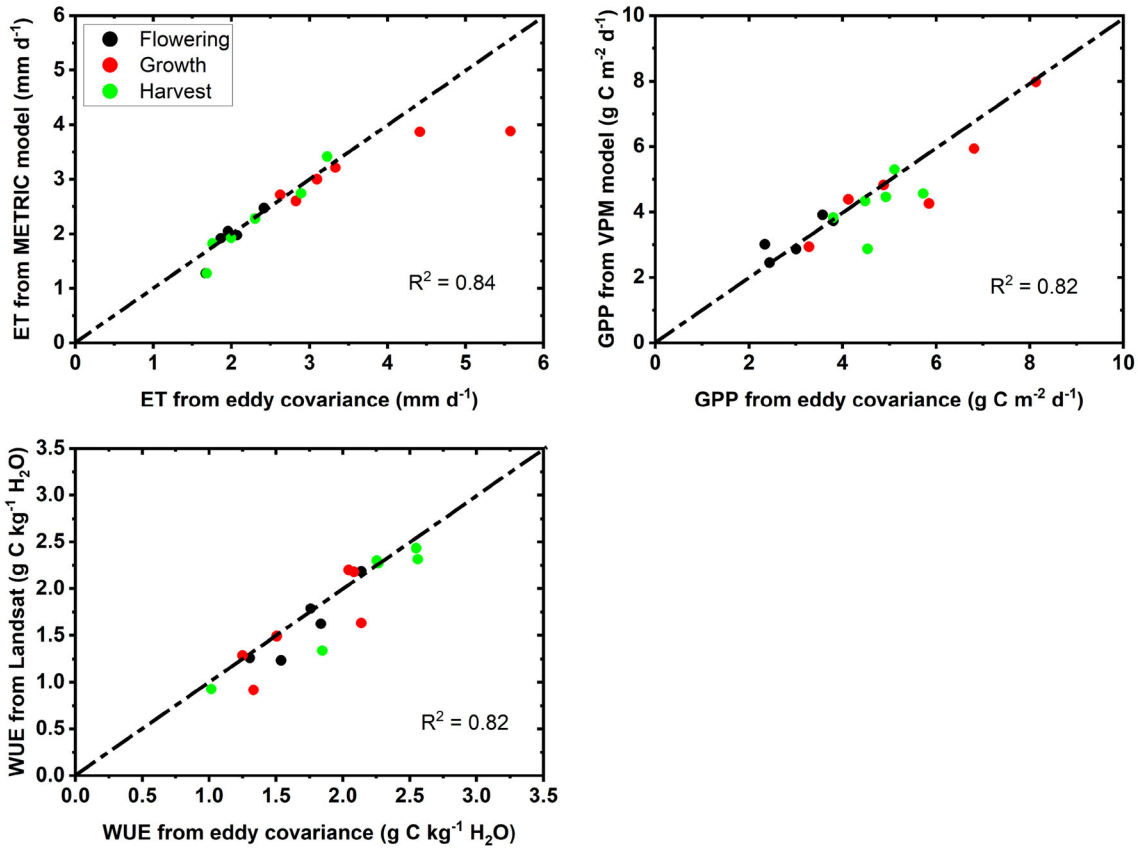

Figure 7. Scatter plots of ET, GPP, and WUE fluxes derived from the EC measurements and Landsat estimates (at the pixel containing flux tower) for different growth stages. A strong positive correlation between the two datasets ($R^2 > 0.80$) confirms the efficiency of Landsat in estimating ET, GPP, and WUE fluxes at the regional scale (crop stages considered include: flowering: April–June, growth: July–October, and harvest: November–December).

water during summer months. During the winter (pre-flowering) season, farmers in the region consciously water stress the orange trees to initiate blooming. This stress results in reduced water uptake, thus decreasing ET. Low GPP during the pre-flowering stage can be attributed to the dormant

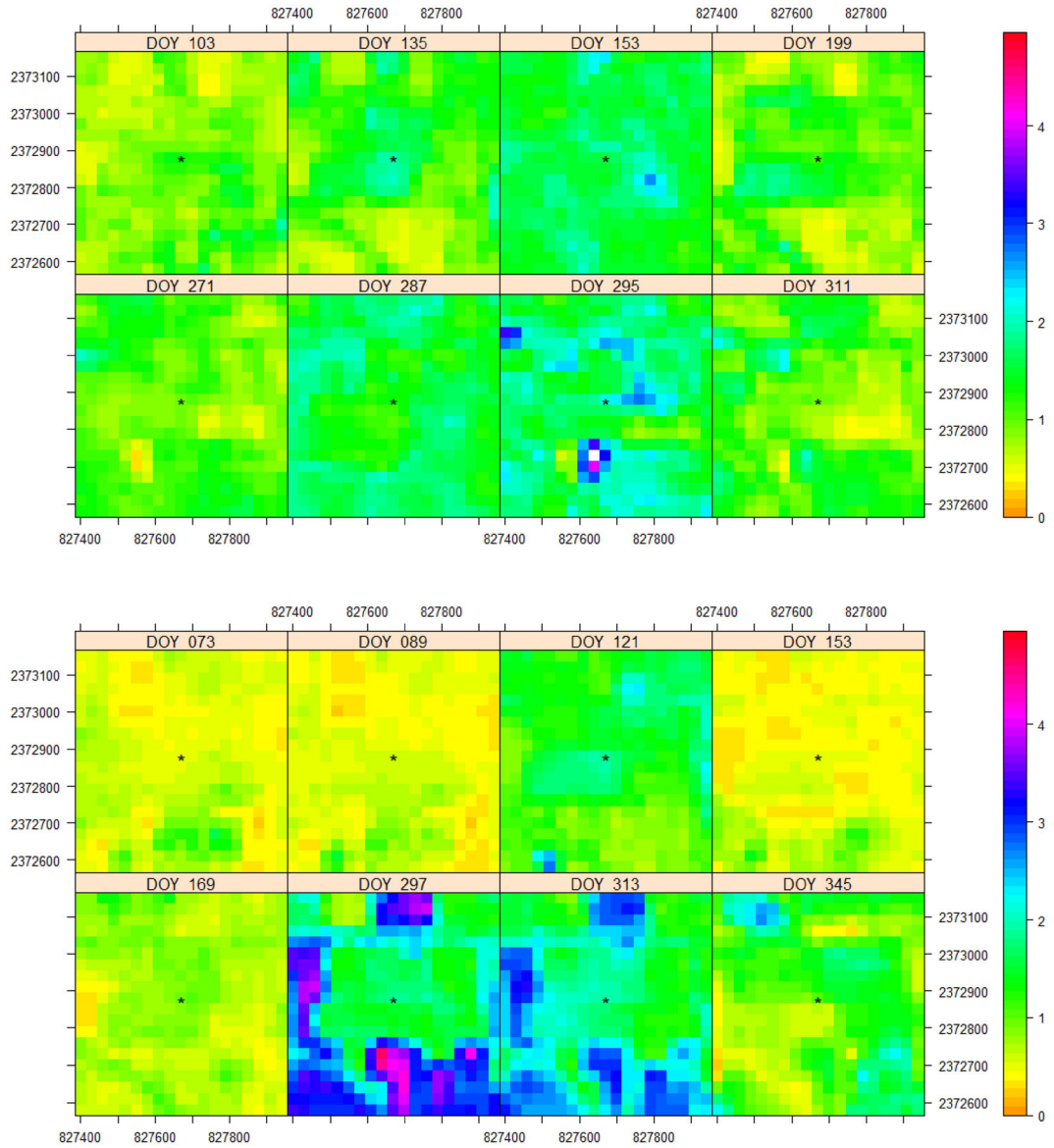

Figure 8. Spatial distribution of Landsat-derived WUE fluxes for the dates of satellite overpass during 2016 (top) and 2017 (bottom). The model domain has an area of 3.6 km^2 (20 × 20 pixels) with flux tower located at the center.

stage of the crop resulting from short and cool days. During the summer (flowering) months, low precipitation combined with high air temperature and VPD resulted in a short-term drought situation. As a result, both carbon assimilation and plant growth were suppressed under combined environment and water stress conditions. Although favorable climate conditions exist during the early growth stage (May-June), insufficient irrigation, and low soil moisture resulted in reduced ET and GPP fluxes (Figure 4). Precipitation paired with soil moisture and radiation caused GPP to be much higher than ET during the fruit development and ripening stages (June-October), leading to an increase in WUE. This result could be due to the decrease in stomatal conductance under high temperature and radiation conditions, which prevented transpiration from becoming much higher than the photosynthesis rate. Meteorological and biophysical parameters strongly influence WUE_E due to their effects on energy partitioning and canopy conductance.

The monthly GPP and ET fluxes strongly agreed with the relative humidity and precipitation patterns, particularly during the early fruit growth stage (July–August). The air temperature-to-GPP

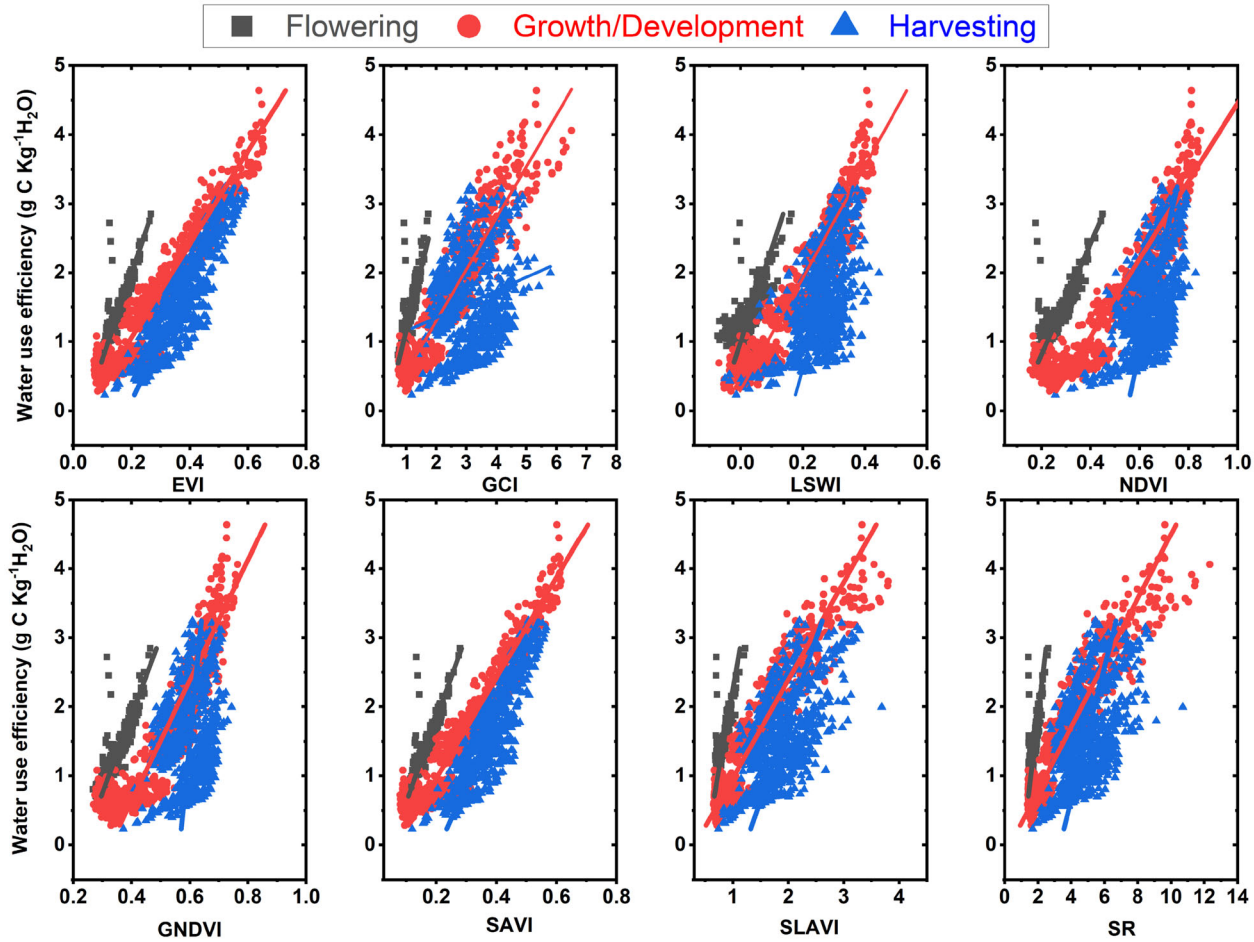

Figure 9. Relationship of Landsat-derived WUE fluxes with various biophysical spectral indices applicable to flowering (WUE_F), growth (WUE_G), and harvest (WUE_H) stages (crop stages considered include: flowering: April–June, growth: July–October, and harvest: November–December).

correlation was observed to be weaker than the VPD-to-ET correlation during the crop cycle. Monthly ecosystem WUE is positively correlated with soil water content and precipitation (Figure 5B, D, F) and negatively correlated with VPD, solar radiation, and air temperature (Figure 5A, C, E). These findings were consistent with the results of other studies performed under temperate climate conditions (Tong and others 2009, 2014b). More than 70% of the variations in the ET, GPP, and WUE fluxes were explained by the seasonal variability in solar radiation, soil moisture, VPD, humidity and precipitation at $P < 0.01$ (data not shown).

The WUE values from the different crop growth stages (1.46–3.49 g C kg^{-1} H_2O) were consistent with those observed in other studies conducted in this region by Panigrahi and Srivastava (2017) as well as the results of a global meta-analysis of citrus water use and yields conducted by Qin and others (2016). Since the studies on WUE fluxes in citrus orchards are limited, we further compared our findings with other crops that use similar techniques. Abraha and others (2016) reported the ecosystem WUE values for annual corn (4.1 g C $kg^{-1}H_2O$) and perennial grassland (2.3 g C kg^{-1} H_2O) in a humid temperate climate. Additionally, Hamilton and others (2015) and Zeri and others (2013) noted that perennial crops exhibit low water use compared to annual crops such as maize (corn) and citrus, which is in agreement with the current findings. Peddinti and Kambhammettu (2019) developed region-specific single and dual crop coefficients for this study area for use with field-scale precision irrigation and management practices. The ET and WUE results from this study can be useful for implementing field-scale irrigation and management practices on a regional scale.

Table 1. Linear Regression Functions Used in Estimating WUE Fluxes from Spectral Indices During Citrus Growth Stages (–)

Spectral index	Flowering stage (n = 400)					Growth stage (n = 680)					Harvest stage (n = 680)				
	Intercept	Slope	R^2	SE	CV	Intercept	Slope	R^2	SE	CV	Intercept	Slope	R^2	SE	CV
EVI	0.039	0.081	0.84	0.002	0.210	0.043	0.147	0.92	0.0003	0.025	0.184	0.113	0.76	0.0003	0.026
GCI	− 0.636	1.801	0.78	0.052	0.231	− 0.193	0.745	0.86	0.030	0.322	0.957	0.195	0.05	0.091	0.623
LSWI	− 0.073	0.073	0.51	0.005	0.201	− 0.036	0.123	0.90	0.002	0.212	0.162	0.061	0.31	0.005	0.202
NDVI	0.099	0.124	0.73	0.005	0.242	0.211	0.177	0.84	0.003	0.199	0.546	0.064	0.26	0.006	0.283
GNDVI	0.233	0.088	0.77	0.003	0.262	0.327	0.114	0.79	0.004	0.252	0.565	0.023	0.05	0.005	0.437
SAVI	0.048	0.082	0.83	0.002	0.211	0.067	0.137	0.91	0.003	0.117	0.211	0.101	0.74	0.003	0.241
SLAVI	0.511	0.216	0.76	0.008	0.323	0.317	0.705	0.90	0.016	0.333	1.222	0.427	0.35	0.034	0.392
SR	1.084	0.489	0.76	0.019	0.442	0.328	2.149	0.88	0.029	0.265	3.318	1.041	0.26	0.061	0.295

(y = slope · x + intercept). Here, y represents WUE and x represents spectral index under consideration.
The robustness of each regression fit is evaluated statistically using correlation coefficient, R^2 (–), standard error, SE (g C kg^{-1} H_2O), and coefficient of variation, CV.

Spectral Dominance of WUE Fluxes

The biophysical spectral indices based on visible, near-infrared, and far-infrared bands of the electromagnetic spectrum are generally associated with plant health status and water stress conditions. Many studies (Jackson 1986; Jackson and others 2004; Zúñiga and others 2016) have suggested that the crop water status and irrigation practices can be estimated purely based on spectral indices such as NDVI and NDWI. During the flowering stage, almost all indices except LSWI were able to explain the WUE dynamics (Figure 9). During the growth stage, all indices performed better, while during the harvest stage, EVI and SAVI were able to capture the WUE dynamics (Table 1). This result confirms that the indices that use the normalized difference of reflectance in red and near-infrared bands can perform better in explaining the WUE dynamics than simple ratio-based or difference-based indices. Overall, Landsat-retrieved EVI and SAVI can be considered as the best surrogates to explain the spatiotemporal dynamics in WUE for citrus orchards of central India. We observed low NDVI during the flowering stage, which can be attributed to the decreased canopy fraction resulting from conscious water stress (Zúñiga and others 2016). In addition, a high bare land fraction during this period might have decreased the NDVI.

Conclusion

Accurate and synoptic quantification of ecosystem WUE is indispensable to implement efficient management strategies in response to natural and anthropogenic stresses. In this study, we present a methodology to reveal the diurnal and seasonal patterns of WUE by combining tower-based (eddy covariance) and satellite-based (Landsat) measurements. Application of the proposed methodology was tested for the citrus orchards of central India using two crop cycle data. During the crop cycle, environmental conditions were observed to influence the photosynthesis and transpiration processes with varying strengths resulting in temporal variations in WUE. Landsat-derived ET (from METRIC), GPP (from VPM), and WUE (GPP/ET) fluxes were observed to be consistent with the EC flux measurements ($R^2 > 0.80$). We concluded that remote sensing-based carbon and water flux estimation methods can be utilized to upscale the ecosystem fluxes in citrus orchards for characterizing regional WUE variability. Our results conclude that EVI and SAVI had higher correlation strengths ($R^2 > 0.75$) with WUE at all growth

stages. We then proposed site-specific empirical relations (between WUE and dominant spectral indices) that can be utilized to evaluate irrigation management practices in response to changing agro-climatic conditions.

ACKNOWLEDGEMENTS

This research is carried as a part of ITRA-Water project that was supported by Media Lab Asia, Ministry of Communications and Information Technology, Government of India. The authors also acknowledge the subject matter expert Dr. Hicke Jeffrey for his critical and valuable comments toward improving the manuscript.

REFERENCES

Abraha M, Gelfand I, Hamilton SK, Shao C, Su YJ, Robertson GP, Chen J. 2016. Ecosystem Water-Use Efficiency of Annual Corn and Perennial Grasslands: Contributions from Land-Use History and Species Composition. Ecosystems 19:1001–12.

Ahongshangbam J, Patel NR, Kushwaha SPS, Watham T, Dadhwal VK. 2016. Estimating Gross Primary Production of a Forest Plantation Area Using Eddy Covariance Data and Satellite Imagery. J Indian Soc Remote Sens 44:895–904.

Allen RG, Tasumi M, Trezza R. 2007. Satellite-Based Energy Balance for Mapping Evapotranspiration with Internalized Calibration (METRIC)—Model. J Irrig Drain Eng 133:380–94.

Bastiaanssen WGM. 2000. SEBAL-based sensible and latent heat fluxes. 229:87–100.

Brümmer C, Black TA, Jassal RS, Grant NJ, Spittlehouse DL, Chen B, Nesic Z, Amiro BD, Arain MA, Barr AG, Bourque CPA, Coursolle C, Dunn AL, Flanagan LB, Humphreys ER, Lafleur PM, Margolis HA, McCaughey JH, Wofsy SC. 2012. How climate and vegetation type influence evapotranspiration and water use efficiency in Canadian forest, peatland and grassland ecosystems. Agric For Meteorol 153:14–30.

Consoli S, Stagno F, Roccuzzo G, Cirelli GL, Intrigliolo F. 2014. Sustainable management of limited water resources in a young orange orchard. Agric Water Manag 132:60–8.

Danelichen VHM, Biudes MS, Velasque MCS, Machado NG, Gomes RSR, Vourlitis GL, Nogueira JS. 2015. Estimating of gross primary production in an Amazon-cerrado transitional forest using MODIS and landsat imagery. An Acad Bras Cienc 87:1545–64.

Dar EA, Brar AS, Singh KB. 2017. Water use and productivity of drip irrigated wheat under variable climatic and soil moisture regimes in North-West, India. Agric Ecosyst Environ 248:9–19.

Dong G, Guo J, Chen J, Sun G, Gao S, Hu L, Wang Y. 2011. Effects of Spring Drought on Carbon Sequestration. Evapotranspiration and Water Use Efficiency in the Songnen Meadow Steppe in Northeast China. 224:211–24.

Fan M, Shen J, Yuan L, Jiang R, Chen X, Davies WJ, Zhang F. 2012. Improving crop productivity and resource use efficiency to ensure food security and environmental quality in China. J Exp Bot 63:13–24.

Gitelson AA, Kaufman YJ, Merzlyak MN. 1996. Use of a green channel in remote sensing of global vegetation from EOS-MODIS. Remote Sens Environ 58:289–98.

Gitelson AA, Peng Y, Masek JG, Rundquist DC, Verma S, Suyker A, Baker JM, Hatfield JL, Meyers T. 2012. Remote estimation of crop gross primary production with Landsat data. Remote Sens Environ 121:404–14.

Gitelson AA, Viña A, Arkebauer TJ, Rundquist DC, Keydan G, Leavitt B. 2003. Remote estimation of leaf area index and green leaf biomass in maize canopies. Geophys Res Lett 30:n/a-n/a.

Gitelson AA, Vina A, Masek JG, Verma SB, Suyker AE. 2008. Synoptic monitoring of gross primary productivity of maize using Landsat data. Ieee Geosci Remote Sens Lett 5:133–7.

Gonzalez-Dugo MP, Neale CMU, Mateos L, Kustas WP, Prueger JH, Anderson MC, Li F. 2009. A comparison of operational remote sensing-based models for estimating crop evapotranspiration. Agric For Meteorol 149:1843–53.

Hamilton SK, Hussain MZ, Bhardwaj AK, Basso B, Robertson GP. 2015. Comparative water use by maize, perennial crops, restored prairie, and poplar trees in the US Midwest. Environ Res Lett 10(6):064015. https://doi.org/10.1088/1748-9326/10/6/064015.

Heinsch FA, Zhao M, Running SW, Kimball JS, Nemani RR, Davis KJ, Bolstad PV, Cook BD, Desai AR, Ricciuto DM, Law BE, Oechel WC, Kwon H, Luo H, Wofsy SC, Dunn AL, Munger JW, Baldocchi DD, Xu L, Hollinger DY, Richardson AD, Stoy PC, Siqueira MBS, Monson RK, Burns SP, Flanagan LB. 2006. Evaluation of remote sensing based terrestrial productivity from MODIS using regional tower eddy flux network observations. IEEE Trans Geosci Remote Sens 44:1908–23.

Huete AR. 1988. A soil-adjusted vegetation index (SAVI). Remote Sens Environ 25:295–309.

Huete AR, Liu HQ, Batchily K, van Leeuwen WJ. 1997. A comparison of vegetation indices over a Global set of TM images for EO -MODIS. Remote Sens Environ 59:440–51.

Ito A, Inatomi M. 2012. Use of a process-based model for assessing the methane budgets of global terrestrial ecosystems and evaluation of uncertainty. Biogeosciences 9:759–73.

Jackson RD. 1986. Remote Sensing of Biotic and Abiotic Plant Stress. Annu Rev Phytopathol 24:265–87. http://www.annualreviews.org/ https://doi.org/10.1146/annurev.py.24.090186.001405.

Jackson TJ, Chen D, Cosh M, Li F, Anderson M, Walthall C, Doriaswamy P, Hunt ER. 2004. Vegetation water content mapping using Landsat data derived normalized difference water index for corn and soybeans. Remote Sens Environ 92:475–82.

Jiang Z, Huete AR, Didan K, Miura T. 2008. Development of a two-band enhanced vegetation index without a blue band. Remote Sens Environ 112:3833–45.

Jordan CF. 1969. Derivation of Leaf-area index from quality of light on the forest floor. Ecology 50:663–6.

Jung M, Reichstein M, Ciais P, Seneviratne SI, Sheffield J, Goulden ML, Bonan G, Cescatti A, Chen J, de Jeu R, Dolman AJ, Eugster W, Gerten D, Gianelle D, Gobron N, Heinke J, Kimball J, Law BE, Montagnani L, Mu Q, Mueller B, Oleson K, Papale D, Richardson AD, Roupsard O, Running S, Tomelleri E, Viovy N, Weber U, Williams C, Wood E, Zaehle S, Zhang K. 2010. Recent decline in the global land evapotranspiration trend due to limited moisture supply. Nature 467:951–4.

Kalfas JL, Xiao X, Vanegas DX, Verma SB, Suyker AE. 2011. Modeling gross primary production of irrigated and rain-fed

maize using MODIS imagery and CO2 flux tower data. Agric For Meteorol 151:1514–28.

Kang X, Hao Y, Cui X, Chen H, Huang S, Du Y, Li W, Kardol P, Xiao X, Cui L. 2016. Variability and changes in climate, phenology, and gross primary production of an alpine wetland ecosystem. Remote Sens 8(5):391.

Kottek M, Grieser J, Beck C, Rudolf B, Rubel F. 2006. World map of the Köppen-Geiger climate classification updated. Meteorol Zeitschrift 15:259–63.

Kuglitsch FG, Reichstein M, Beer C, Carrara A, Ceulemans R, Granier A, Janssens IA, Koestner B, Lindroth A, Loustau D, Matteucci G, Montagnani L, Moors EJ, Papale D, Pilegaard K, Rambal S, Rebmann C, Schulze ED, Seufert G, Verbeeck H, Vesala T, Aubinet M, Bernhofer C, Foken T, Grünwald T, Heinesch B, Kutsch W, Laurila T, Longdoz B, Miglietta F, Sanz MJ, Valentini R. 2008. Characterisation of ecosystem water-use efficiency of european forests from eddy covariance measurements. Biogeosciences Discuss 5:4481–519.

Law B, Falge E, Gu L, Baldocchi D, Bakwin P, Berbigier P, Davis K, Dolman A, Falk M, Fuentes J, Goldstein A, Granier A, Grelle A, Hollinger D, Janssens I, Jarvis P, Jensen N, Katul G, Mahli Y, Matteucci G, Meyers T, Monson R, Munger W, Oechel W, Olson R, Pilegaard K, Paw UK, Thorgeirsson H, Valentini R, Verma S, Vesala T, Wilson K, Wofsy S. 2002. Environmental controls over carbon dioxide and water vapor exchange of terrestrial vegetation. Agric For Meteorol 113:97–120.

Li Z, Yu G, Xiao X, Li Y, Zhao X, Ren C, Zhang L, Fu Y. 2007. Modeling gross primary production of alpine ecosystems in the Tibetan Plateau using MODIS images and climate data. Remote Sens Environ 107:510–19.

Liu X, Chen X, Li R, Long F, Zhang L, Zhang Q, Li J. 2017. Water-use efficiency of an old-growth forest in lower subtropical China. Sci Rep 7:42761.

Liu Z, Wang L, Wang S. 2014. Comparison of different GPP models in China using MODIS image and ChinaFLUX data. Remote Sens 6:10215–31.

Lloyd J, Taylor J. 1994. On the temperature dependence of soil respiration. Funct Ecol 8:315–23.

Lymburner L, Beggs P, Jacobson C. 2000. Estimation of canopy-average surface-specific leaf area using Landsat TM data. Photogramm Eng Remote Sens 66:183–91.

Madugundu R, Al-Gaadi KA, Tola EK, Kayad AG, Jha CS. 2017. Estimation of gross primary production of irrigated maize using Landsat-8 imagery and Eddy Covariance data. Saudi J Biol Sci 24:410–20.

Niu S, Xing X, Zhang Z, Xia J, Zhou X, Song B, Li L, Wan S. 2011. Water-use efficiency in response to climate change: From leaf to ecosystem in a temperate steppe. Glob Chang Biol 17:1073–82.

Olmedo GF, Ortega-Farias S, de la Fuente-Sáiz D, Fonseca-Luego D, Fuentes-Penailillo F. 2016. water: Tools and Functions to Estimate Actual Evapotranspiration Using Land Surface Energy Balance Models in R. R J 8:352–69.

Osmond B, Ananyev G, Berry J, Langdon C, Kolber Z, Lin G, Monson R, Nichol C, Rascher U, Schurr U, Smith S, Yakir D. 2004. Changing the way we think about global change research: Scaling up in experimental ecosystem science. Glob Chang Biol 10:393–407.

Panigrahi P, Srivastava AK. 2017. Water and nutrient management effects on water use and yield of drip irrigated citrus in vertisol under a sub-humid region. J Integr Agric 16:1184–94.

Peddinti SR, Kambhammettu BP. 2019. Dynamics of crop coefficients for citrus orchards of central India using water balance and eddy covariance flux partition techniques. Agric Water Manag 212:68–77. https://doi.org/10.1016/j.agwat.2018.08.027.

Peddinti SR, Kambhammettu BVNP, Ranjan S, Suradhaniwar S, Badnakhe MR, Adinarayana J, Gade RM. 2018. Modeling Soil–Water–Disease Interactions of Flood-Irrigated Mandarin Orange Trees: Role of Root Distribution Parameters. Vadose Zo J 17:0. https://dl.sciencesocieties.org/publications/vzj/abstracts/17/1/170129.

Ponton S, Flanagan LB, Alstad KP, Johnson BG, Morgenstern K, Kljun N, Black TA, Barr AG. 2006. Comparison of ecosystem water-use efficiency among Douglas-fir forest, aspen forest and grassland using eddy covariance and carbon isotope techniques. Glob Chang Biol 12:294–310.

Prince SD, Goward SN. 1996. International Journal of Remote Sensing Evaluation of the NOAA / NASA Pathfinder AVHRR Land Data Set for global primary production modelling. INT J Remote Sens 17:217–21.

Qin W, Assinck FBT, Heinen M, Oenema O. 2016. Water and nitrogen use efficiencies in citrus production: A meta-analysis. Agric Ecosyst Environ 222:103–11.

Raich AJW, Rastetter EB, Melillo JM, Kicklighter DW, Steudler PA, Grace AL, Iii BM, Vörösmarty CJ, Applications SE, Nov N. 1991. Potential net primary productivity in South America: Application of a global model. Ecol Appl 1:399–429.

Reichstein M, Ciais P, Papale D, Valentini R, Running S, Viovy N, Cramer W, Granier A, Ogée J, Allard V, Aubinet M, Bernhofer C, Buchmann N, Carrara A, Grünwald T, Heimann M, Heinesch B, Knohl A, Kutsch W, Loustau D, Manca G, Matteucci G, Miglietta F, Ourcival JM, Pilegaard K, Pumpanen J, Rambal S, Schaphoff S, Seufert G, Soussana JF, Sanz MJ, Vesala T, Zhao M. 2007. Reduction of ecosystem productivity and respiration during the European summer 2003 climate anomaly: A joint flux tower, remote sensing and modelling analysis. Glob Chang Biol 13:634–51.

Roccuzzo G, Villalobos FJ, Testi L, Fereres E. 2014. Effects of water deficits on whole tree water use efficiency of orange. Agric Water Manag 140:61–8.

Rodda SR, Thumaty KC, Jha CS, Dadhwal VK. 2016. Seasonal Variations of Carbon Dioxide, Water Vapor and Energy Fluxes in Tropical Indian Mangroves. Forestes 7:1–18.

Rouse JW, Hass RH, Schell JA, Deering DW. 1973. Monitoring vegetation systems in the great plains with ERTS. Third Earth Resour Technol Satell Symp 1:309–17.

Ruimy A, Jarvis PG, Baldocchi DD, Saugier B. 1995. CO_2 fluxes over plant canopies and solar radiation: A review. Adv Ecol Res 26:1–68.

Running SW, Thornton PE, Nemani RR, Glassy JM. 2000. Global terrestrial gross and net primary productivity from the earth observing system. In: Sala O, Jackson R, Mooney H, Eds. Methods in Ecosystem Science. New York: Springer-Verlag.

Song Q-H, Fei X-H, Zhang Y-P, Sha L-Q, Liu Y-T, Zhou W-J, Wu C-S, Lu Z-Y, Luo K, Gao J-B, Liu Y-H. 2017. Water use efficiency in a primary subtropical evergreen forest in Southwest China. Sci Rep 7:43031.

Souza MC, Biudes MS, de Morais Danelichen VH, Machado NG, de Musis CR, Vourlitis GL, de Souza Nogueira J. 2014. Estimation of gross primary production of the Amazon-Cerrado transitional forest by remote sensing techniques. Rev Bras Meteorol 29:01–12.

Tang X, Ding Z, Li H, Li X, Luo J, Xie J, Chen D. 2015a. Characterizing ecosystem water-use efficiency of croplands with eddy covariance measurements and MODIS products. Ecol Eng 85:212–17.

Tang X, Li H, Desai AR, Nagy Z, Luo J, Kolb TE, Olioso A, Xu X, Yao L, Kutsch W, Pilegaard K, Köstner B, Ammann C. 2015b. How is water-use efficiency of terrestrial ecosystems distributed and changing on Earth? Sci Rep 4:7483.

Tang X, Wang Z, Xie J, Liu D, Desai AR, Jia M, Dong Z, Liu X, Liu B. 2013. Monitoring the seasonal and interannual variation of the carbon sequestration in a temperate deciduous forest with MODIS time series data. For Ecol Manage 306:150–60.

Tejero IG, Zuazo VHD, Bocanegra JAJ, Fernández JLM. 2011. Improved water-use efficiency by deficit-irrigation programmes: Implications for saving water in citrus orchards. Sci Hortic (Amsterdam) 128:274–82.

Tong X, Li J, Yu Q, Lin Z. 2014a. Biophysical Controls on Light Response of Net CO2 Exchange in a Winter Wheat Field in the North China Plain. PLoS One 9:e89469.

Tong X, Zhang J, Meng P, Li J, Zheng N. 2014b. Ecosystem water use efficiency in a warm-temperate mixed plantation in the North China. J Hydrol 512:221–8. https://doi.org/10.1016/j.jhydrol.2014.02.042.

Tong XJ, Li J, Yu Q, Qin Z. 2009. Ecosystem water use efficiency in an irrigated cropland in the North China Plain. J Hydrol 374:329–37. https://doi.org/10.1016/j.jhydrol.2009.06.030.

Turner DP, Ritts WD, Cohen WB, Gower ST, Running SW, Zhao M, Costa MH, Kirschbaum AA, Ham JM, Saleska SR, Ahl DE. 2006. Evaluation of MODIS NPP and GPP products across multiple biomes. Remote Sens Environ 102:282–92.

Turner DP, Ritts WD, Cohen WB, Maeirsperger TK, Gower ST, Kirschbaum AA, Running SW, Zhao M, Wofsy SC, Dunn AL, Law BE, Campbell JL, Oechel WC, Kwon HJ, Meyers TP, Small EE, Kurc SA, Gamon JA. 2005. Site-level evaluation of satellite-based global terrestrial gross primary production and net primary production monitoring. Glob Chang Biol 11:666–84.

Wagle P, Kakani VG. 2012. Growing season variability in evapotranspiration, ecosystem water use efficiency, and energy partitioning in switchgrass.

Wang Z, Xiao X, Yan X. 2010. Modeling gross primary production of maize cropland and degraded grassland in northeastern China. Agric For Meteorol 150:1160–7.

Wu C, Munger JW, Niu Z, Kuang D. 2010. Comparison of multiple models for estimating gross primary production using MODIS and eddy covariance data in Harvard Forest. Remote Sens Environ 114:2925–39.

Xiao X, Hollinger D, Aber J, Goltz M, Davidson EA, Zhang Q, Moore B. 2004a. Satellite-based modeling of gross primary production in an evergreen needleleaf forest. Remote Sens Environ 89:519–34.

Xiao X, Zhang Q, Braswell B, Urbanski S, Boles S, Wofsy S, Moore B, Ojima D. 2004b. Modeling gross primary production of temperate deciduous broadleaf forest using satellite images and climate data. Remote Sens Environ 91:256–70.

Xiao X, Zhang Q, Hollinger D, Aber J, Berrien M. 2005. Modeling gross primary production of an evergreen needleleaf forest using modis and climate data. Ecol Appl 15:954–69.

Yan H, Fu Y, Xiao X, Huang HQ, He H, Ediger L. 2009. Modeling gross primary productivity for winter wheat-maize double cropping system using MODIS time series and CO2 eddy flux tower data. Agric Ecosyst Environ 129:391–400.

Yu G, Song X, Wang Q, Liu Y, Guan D, Yan J, Sun X, Zhang L, Wen X. 2008. Water-use efficiency of forest ecosystems in eastern China and its relations to climatic variables. New Phytol 177:927–37.

Zeri M, Hussain MZ, Anderson-Teixeira KJ, Delucia E, Bernacchi CJ. 2013. Water use efficiency of perennial and annual bioenergy crops in central Illinois. J Geophys Res Biogeosciences 118:581–9.

Zhang J, Hu Y, Xiao X, Chen P, Han S, Song G, Yu G. 2009. Satellite-based estimation of evapotranspiration of an old-growth temperate mixed forest. Agric For Meteorol 149:976–84.

Zhang J, Ren W, An P, Pan Z, Wang L, Dong Z, He D, Yang J, Pan S, Tian H. 2015. Responses of crop water use efficiency to climate change and agronomic measures in the semiarid area of Northern China. PLoS One 10:1–22.

Zhang Y, Xiao X, Jin C, Dong J, Zhou S, Wagle P, Joiner J, Guanter L, Zhang Y, Zhang G, Qin Y, Wang J, Moore B. 2016. Consistency between sun-induced chlorophyll fluorescence and gross primary production of vegetation in North America. Remote Sens Environ 183:154–69.

Zhao F-H, Yu G-R, Li S-G, Ren C-Y, Sun X-M, Mi N, Li J, Ouyang Z. 2007. Canopy water use efficiency of winter wheat in the North China Plain. Agric Water Manag 93:99–108.

Zhao M, Running SW. 2009. Drought-induced reduction in global terrestrial net primary production from 2000 through 2009. Science 80(329):940–3.

Zúñiga CE, Khot LR, Jacoby P, Sankaran S. 2016. Remote sensing based water-use efficiency evaluation in sub-surface irrigated wine grape vines. In: Autonomous Air and Ground Sensing Systems for Agricultural Optimization and Phenotyping. Vol. 9866, p. 986600.